

I. IMPLEMENTATION EXAMPLES

In this section, we provided detailed ESI implementation procedures on epileptic EEG data, with the hope of demonstrating and facilitating the application of ESI methods in realistic cases. The epileptic data were collected from a patient suffering from focal epilepsy, which are publicly available at¹. A total of 58 epileptiform discharges (spikes) are provided, and the clinical evidence showed the origin of the epilepsy located at left frontal lobe [1]. We elaborate on the implementation details regarding source reconstruction of epileptic activities using four ESI algorithms based on DS model, given the potential benefits on estimating source extents of DS model over ECD model. These algorithms involve LORETA [2], sparse bayesian learning (SBL) [3], STAR [4], VSSI-GGD [5], and ResNet-LSTM model [6], which represent the smoothness-constrained MN family, sparsity-constrained method, spatio-temporal constrained method, the gradient domain-constrained method, and deep learning method respectively.

A. Data Processing

The procedure involves preprocessing of epileptic EEG data to extract seizure-related spike signals, as well as to construct the lead-field matrix and head model from patient-specific sMRI. We followed the protocols outlined in Brainstorm tutorial to get the spikes, lead-field matrix and head model⁽²⁾. The processing steps are briefly introduced here:

1) Artifact Removal and Re-reference: The 29-channel EEG data are band-pass filtered into [0.5, 80] Hz and subsequently re-referenced using average referenced. ICA is then performed to remove ocular artifacts.

2) Spike Extraction and Averaging: Spike activities are extracted from -0.3s to 0.5s relative to the onset of spike events. A total number of 58 spikes are identified and extracted. To enhance SNR of the epileptic activities, spikes are averaged under three trial conditions: the first 10 (Trials = 10), 30 (Trials = 30), and 58 (Trials = 58) spikes to account for different signal SNRs.

3) Lead-Field Matrix and Head Model: The calculation of lead-field matrix and head model follows the standard pipelines and settings described in the Brainstorm tutorial. The cortex is downsampled into 6006 dipoles in this section, with the orientation of each dipole being fixed perpendicular to the cortex surface. The lead-field matrix is average re-referenced.

4) Depth Compensation: Depth compensation is implemented proportional to the square of norm of lead-field matrix. This adjustment could mitigate the bias of ESI results due to depth of source:

$$\Psi = \text{diag}(\Psi_i), (\Psi_i = \frac{1}{\|L_i\|_2}) \quad (1)$$

$$L = L \times \Psi$$

5) Noise Whitening: Noise whitening could mitigate the influence of various noise levels on different electrodes and normalize the noise distribution. Typically, the noise covariance matrix could be estimated from baseline signals, and then whitening the data and lead-field matrix prior to ESI. For this analysis, the noise covariance matrix is estimated using data from -0.3s to -0.1s relative to the spike event. Given that the spike data have been averaged across multiple trials to

cancel the noise, and with the limited baseline data available, the estimation of noise covariance matrix may be biased and the commonly-used whitening is not appropriate. Instead, the noise matrix is enforced to be diagonal, with each diagonal element being proportional to the inverse of power of baseline activities from corresponding channel. The primary objective is to enforce uniform noise levels across all channels:

$$\Sigma_{noise}^{-1} = \text{diag}\left(\frac{1}{\sigma_i}\right), (\sigma_i = \text{std}(B(i, Baseline))) \quad (2)$$

$$B = \Sigma_{noise}^{-1} \times B, L = \Sigma_{noise}^{-1} \times L,$$

B. Epilepsy Source Imaging

Once the data have been processed, ESI methods are applied to reconstruct the epileptic sources.

1) Source Imaging Using LORETA method: LORETA is one of the widely-explored MN methods that enforces spatial smoothness through incorporation of surface laplacian operator into M :

$$M = I - \tau \mathcal{N},$$

$$\mathcal{N}_{i,j} = \begin{cases} \frac{1}{|\mathcal{N}_i|} & \text{if } j \in \mathcal{N}_i \\ 0 & \text{others} \end{cases} \quad (3)$$

where \mathcal{N}_i denotes the neighbors of i^{th} dipole and $|\mathcal{N}_i|$ is the number of elements in \mathcal{N}_i , $\tau < 1$ is a constant for stability of calculation and is set to 0.99 here.

The choice of regularization parameter λ is critical for source reconstruction, as it governs the balance between the fidelity to the observed data and the smoothness enforced on the solution. Several strategies can be used to determine λ . First, L-curve approach can be adopted to select the λ objectively to balance the error between data-fit term and regularization term. Besides, λ can be automatically updated under bayesian framework, wherein the LORETA is viewed as a specialized instance of SBL method [7]. In the context of MN family, the parameter can also be adjusted based on the SNR of data. Specifically, the SNR is defined as: $\text{SNR}^2 \propto \frac{\text{trace}(L R_S L^\top)}{\text{trace}(\Sigma_\epsilon)}$, where R_S is the source covariance matrix, $L^\top R_S L$ measures the power of clean data generated by the sources. The λ can be determined from:

$$\lambda \propto \frac{1}{\text{SNR}^2} \frac{\text{trace}(L(M^\top M)^{-1} L^\top)}{\text{trace}(\Sigma_\epsilon)}, \quad (4)$$

if we could get a proper estimation of SNR. In this section, we calculate λ as:

$$\lambda = k \times \frac{\text{trace}(L(M^\top M)^{-1} L^\top)}{\text{trace}(\Sigma_\epsilon)} \quad (5)$$

where $\frac{1}{k} = 16/36/81$ is set empirically for trials= 10/30/58. The procedure is listed as follow:

- **Require:** processed EEG data B and lead-field matrix L , cortex adjacent matrix
- calculate M, λ according to Eq. 3, Eq. 4 respectively
- calculate ESI results.

2) Source Imaging Using SBL method: In this analysis, we adopt SBL method to simultaneously estimate source and noise time course according to EBI-Convex algorithm, which assumes Gaussian prior distribution for both source and noise

¹<https://neuroimage.usc.edu/bst/download.php>

²<https://neuroimage.usc.edu/brainstorm/Tutorials/Epilepsy>

activity:

$$\begin{aligned} B &= [L \quad A] \begin{bmatrix} S \\ u \end{bmatrix} + \epsilon = FX + \epsilon \\ p(B|X) &\propto \exp\left(-\frac{1}{2}\|B - FX\|_{\Sigma_\epsilon^{-1}}\right) \\ p(X|\gamma) &\propto \exp\left(-\frac{1}{2}\|X\|_{\text{diag}(\gamma)}\right), \end{aligned} \quad (6)$$

where u is the unknown noise series, ϵ is a residual term that also assumed to be Gaussian distributed. One advantage of this method is its user-friendly setup as only the prior covariance for residual term is required, which can be a small value to ensure stability. In this analysis, we set the covariance as $10^{-6} \times I$, and the algorithm learns hyperparameters automatically from data. The procedure is:

- **Require:** B and L
- specify residual covariance as $10^{-6} \times I$
- calculate ESI results using SBL

3) Source Imaging Using STAR: The STAR method incorporates spatiotemporal constraints to reconstruct source activities in a data-driven manner. The surface laplacian operator used in LORETA is incorporated to enforce spatial smoothness. For the temporal constraint, the STAR incorporates TBFs Φ derived from singular value decomposition (SVD) of EEG data are used. Specifically, given the decomposition $B = UDV^\top$ of EEG data, we select the first 2 rows of V^\top corresponding to the largest values of D as the initial TBFs:

$$\begin{aligned} B &= UDV^\top, \quad \text{Ind} = \text{sort}(D, \text{'descend'}) \\ V &= V(:, \text{Ind}), \quad \Phi = V(:, [1, 2])^\top \end{aligned} \quad (7)$$

The algorithm is designed to learn hyperparameters automatically from data, and it should converge within 50 iterations. The procedure is:

- **Require:** B , L , cortex adjacent matrix
- calculate M , Φ according to Eq. 3, Eq. 7 respectively
- calculate ESI results using STAR

4) Source Imaging Using VSSI-GGD: VSSI-GGD method addresses the the total-variation problem for ESI:

$$\begin{aligned} \arg \min_S & \|B - LS\|_{Fro} + \alpha \|Vs\|_{2,1} \\ V &= \begin{bmatrix} v_{11} & v_{12} & \cdots & v_{1n} \\ v_{21} & v_{22} & \cdots & v_{2n} \\ \vdots & \vdots & \ddots & \vdots \\ v_{p1} & v_{p2} & \cdots & v_{pn} \end{bmatrix}, \end{aligned} \quad (8)$$

where V is the discrete gradient operator to transform the S from source domain into gradient domain, $v_{ij} = 1$, $v_{ik} = -1$ if dipole j, k share the i^{th} edge and $v_{ij} = 0$ otherwise. This method incorporates sparse constraint in the gradient domain to produce clear boundaries between source and background activities. Additionally, TBFs are employed to reconstruct temporal dynamics of epileptic source activity. To obtain robust reconstruction of source extents, further processing of the original EEG is required to extract activities of interest. Specifically, the original EEG data are decomposed into source components using source separation techniques such as PCA/ICA, and components related to the epilepsy are selected to reconstruct the signals. In this analysis, we adopt PCA for data decomposition, and select the first two dominant principle components for data reconstruction since they contains most epileptic activities. The TBFs are obtained as Eq. 7. Owing to

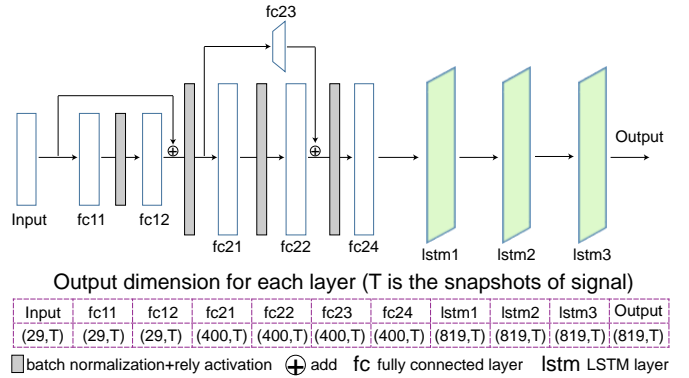


Fig. 1. The architecture of the used ResNet-LSTM

the orthogonality of TBFs, the implementation is equivalent to projecting the data into subspace spanned by the TBFs: $B = \hat{B} \times (\Phi^\top \Phi)$. The procedure is:

- **Require:** B , L , cortex adjacent matrix
- calculate transformation matrix according to Eq. 8
- calculate Φ according to Eq. 7, project the data $B = B \times \Phi^\top$
- calculate spatial weights \hat{S} using VSSI-GGD, $S = \hat{S} \times \Phi$

5) Source Imaging Using ResNet-LSTM: We also incorporate a deep learning method for solving the ESI. In this analysis, we adopt the network architecture ResNet-LSTM that composed of ResNet and LSTM according to [6]. The structure of ResNet-LSTM is depicted in Fig. 1. Initially, the cortex is segmented into 819 non-overlapped patches, and simulated source activities are generated subsequently to train the network. Note that the generated training data could significantly influence the performance of DL model in ESI applications. However, the optimization of the training data generation process is beyond the scope of this section. We adhere to a similar procedure for data generation as described in [8], and we restrict the training data to be single-patch source activities (details regarding the generation of training data could be found in [6], [8]). The loss function of ResNet-LSTM is the mean square error between simulated and reconstructed sources. Through minimizing the loss function until convergence, the trained DL model can estimate the source signals directly from the EEG signals. The procedure is:

- **Require:** B , L
- generate training data using L
- train the ResNet-LSTM
- calculate source activity S using trained ResNet-LSTM with B as input.

C. Visualization of ESI results

The resulted source energy distributions for these representative methods under various SNRs are provided in Fig. 2. Threshold strategy is employed for better presentation purpose. Specifically, thresholds are set as follows:

1) LORETA: 50% of maximum energy for LORETA to address the tendency toward overly-smoothed results.

2) SBL, STAR, and ResNet-LSTM: The thresholds for SBL, STAR, and ResNet-LSTM are based on otsu's method [9].

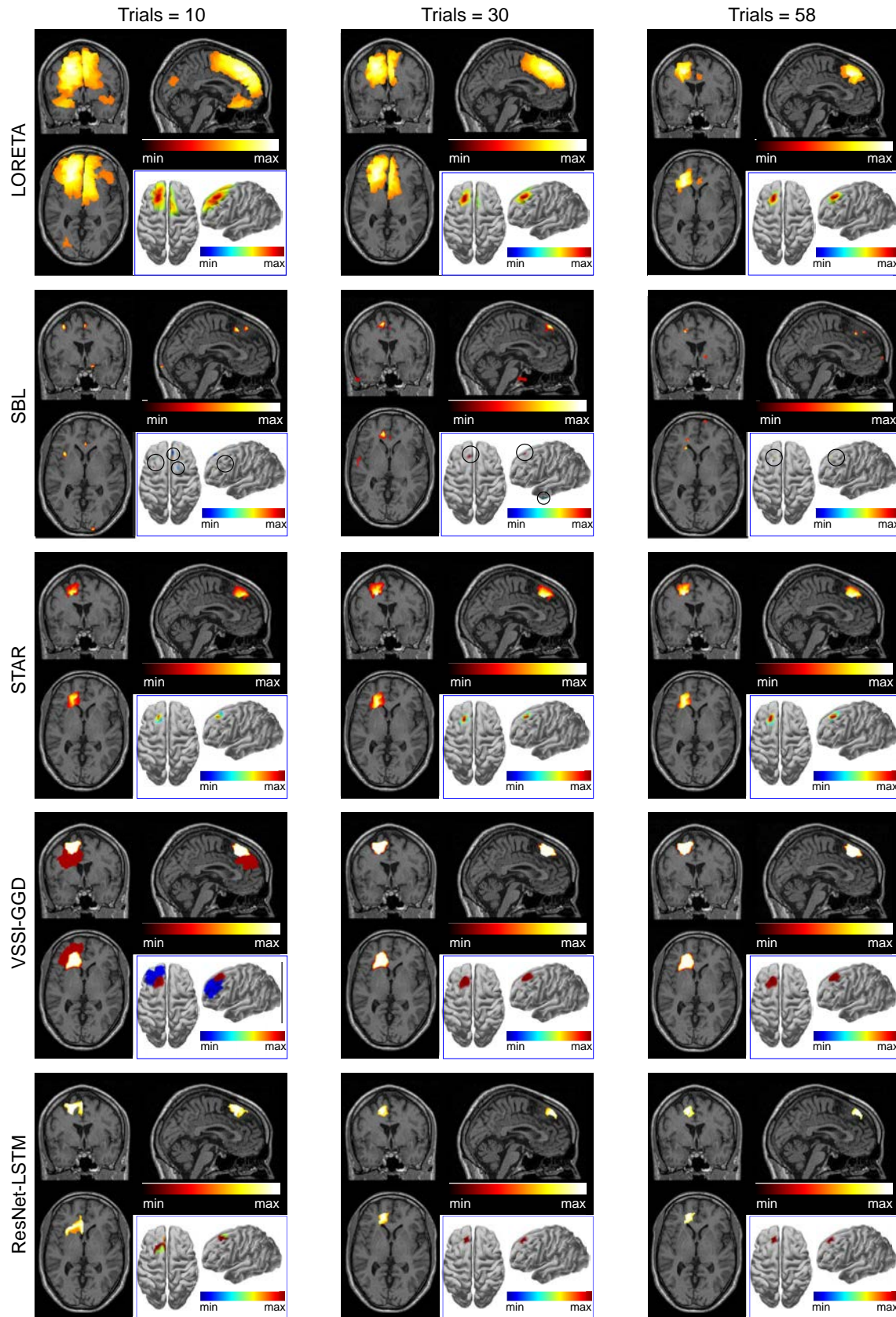


Fig. 2. ESI results of epilepsy from four algorithms under various SNRs

3) VSSI-GGD: The VSSI-GGD could produce clear boundaries between active and non-active sources, thus no threshold is needed mathematically. Here we set a small values (5% of maximum energy) as threshold to avoid the background activities and noise.

Additionally, we present the ESI results projected onto patient-specific sMRI, along with the original results on cortex surface (displayed in the lower right). Both presentations maintain identical settings except that they use different colorbar for better visualization. All employed methods demonstrate consistent estimation of the epilepsy source, and improvement of the SNR could enhance their performance. The LORETA tends to overestimate the extent of source regions, and improvements in SNR helps to refine the reconstruction of source areas. While different choice of λ would influence source estimation, our findings indicate that the above-mentioned three strategies yield similar ESI results (data not shown). The SBL yields focal results that predominantly locate within the epileptic zones. The results offer valuable insights into source locations, but provide little information on source extents. With the same spatial constraints as LORETA, the STAR method leads to smoother estimations of source distribution but exhibits less spatial blurring than LORETA. Nonetheless, threshold is also required to determine the source extents. On the other hand, the VSSI-GGD is able to produce distinguish boundaries between epilepsy and background activities. Notably, the extraction of epilepsy-related components (described in VII.B (4)) is crucial for estimating source extents. However, in the scenarios where the desired activity is hard to extract, e.g., in the case of single trial EEG where the SNR is low, the performance of VSSI-GGD is observed to decline significantly. Finally, the ResNet-LSTM facilitates accurate source estimations significantly faster than traditional ESI methods that employ advanced constraints. However, the design of the network architecture and the generation of training data is crucial for ESI performance. For instance, the segmentation of cortex for data generation, as applied in this analysis, would significantly affect the spatial extents of estimated sources. Alternatively, DL model can also be trained to predict source activities for each dipole and automatically reconstruct source extents. Additionally, it is important to recognize that the trained model approximates the inverse solution for a specific lead-field matrix. Consequently, retraining of the model is required to maintain accuracy in source estimation for a different lead-field matrix.

II. PRACTICAL SELECTION OF HYPERPARAMETERS

The practical efficacy of E/MEG source imaging algorithms is heavily dependent on the selection of hyperparameters. This section outlines key tunable parameters and tuning strategies for common algorithm families, including regularization parameter, depth weighting, noise covariance inference, and data covariance estimation.

The regularization parameter, often denoted as λ , serves to balance the solution between data-fit and prior constraints. It typically appears in the form of $\mathcal{F}(B, L, S) + \lambda\mathcal{R}(S)$, where $\mathcal{F}(B, L, S)$ represents the data-fit term and $\mathcal{R}(S)$ denotes the regularization term. The optimal value of λ can vary significantly depending on practical settings such as the scale of the lead-field matrix and signal strength. A small value is often employed to stabilize the solution. Common strategies to determine the optimal λ include:

- **L-curve analysis:** his method identifies the "knee" point, which represents an optimal balance between the data fit and the regularization norm
- **Generalized Cross-Validation:** This strategy optimizes λ by minimizing a predictive error criterion.
- **SNR-based analysis:** For MNE methods, λ can be estimated based on SNR (refer to Eq. (4)-(5)).
- **Empirical Bayes learning:** For MNE methods, the ESI problem can be solved by maximizing a posterior (MAP) distribution with a Gaussian prior, allowing the hyperparameter λ to be updated directly from data [7].
- **Information criteria:** Criteria such as AIC (Akaike Information Criterion) and BIC (Bayesian Information Criterion) can guide the selection of λ for sparsity-based methods.

The Depth-weighting is often applied to assign higher weights to deep sources, thereby mitigating depth bias. A common approach to construct weights is based on the norm of leadfield matrix, where a larger norm indicates a shallower source. The weighting matrix W is configured as a diagonal matrix, with its elements $W_{i,i} \propto 1/\text{norm}(L_{:,i})^\alpha$. The exponent value α dictates the strength of weighting, commonly ranging from 1 to 2 [10]. Besides, the estimated noise covariance in the source space can be used to standardize the results to compensate the depth bias, as seen in implementations like dSPM and sLORETA.

The noise covariance Σ_n is used to standardize the signals to ensure all electrodes exhibit the same noise level. The Σ_n can be estimated from baseline signal: in MEG, this might involve data collected in an empty room, while in EEG, it refers to periods unrelated to the activity of interest. Recent research has also explored data-driven estimation of Σ_n directly from the signal of interest based on sparse Bayesian learning [11]. The data covariance Σ_B is a crucial component in adaptive methods such as Beamforming. In addition to empirical covariance estimation (e.g., Oracle methods), sparse Bayesian learning has been adopted to estimate the model covariance [12]. These parameters have been summarized in Table I.

Deep learning (DL) models have been increasingly applied to solve the ESI problem. To effectively reconstruct source activity using DL models, it is crucial to carefully consider components such as the model architectures, loss functions, training data, and optimization strategies. Given the rapid growth of DL-based ESI and the still-evolving nature of this field, recent advances in these aspects are systematically summarized in Table II, based on representative works.

III. DEPTH BIAS EVALUATION FOR MN METHODS

The widely-used MN methods are inherently biased towards shallow source. To address this, various strategies have been proposed to compensate for deep sources, including depth-weighting (e.g., as implemented in weighted MNE) and noise-based standardization (e.g., as implemented in sLORETA and dSPM). In this section, the spatial precision and resolution (indicated by DLE and SD) versus depth bias are quantitatively evaluated. Four MN methods were adopted in this experiment:

- LORETA: Laplacian operator is included in the regularization term, and no depth weighting is incorporated in this evaluation.
- weighted MNE (abbreviated as MNE): a diagonal depth-weighting matrix W is included in the regularization term, with $W_{i,i} = 1/(||L_i||_2^2)^{0.5}$.

TABLE I
KEY TUNABLE PARAMETERS IN TRADITIONAL ESI ALGORITHMS

Tunable Parameters	Algorithm Category	Typical Range / Tuning Strategy
Regularization parameter λ	$\mathcal{F}(B, L, S) + \lambda\mathcal{R}(S)$	L-curve analysis Generalized cross-validation SNR-based analysis (for MN families, such as MNE) Empirical Bayes learning (for MN families) Information Criteria (e.g., AIC and BIC, for sparse solution such as MxNE)
Depth weighting W	Almost all $\mathcal{R}(WS)$	$W_{ii} \propto 1/\text{norm}(L_{:,i})^\alpha$ (α can be determined through cross-validation, typically $\in [1, 2]$) Noise-based standardization
Noise covariance Σ_n	$\ B - LS\ _{\Sigma_n}^2 + \mathcal{R}(S)$	Inferred from baseline (can be diagonal) Data-driven estimation via Bayesian learning [11]
Data covariance Σ_B	Beamforming	Empirical Estimation: $\Sigma_B = BB^\top + \beta I$ Sparse Bayesian learning (model covariance) [12]

TABLE II
PRACTICAL DETAILS ON SEVEN REPRESENTATIVE DL-BASED ESI

Model	Architecture	Training Data	Loss design	Optimization
DeepSIF [6]	Residual network & LSTM	Simulated data by neural mass models	$\ S_g - S_{re}\ _F^2$	Adam optimizer, learning rate: 3e-4, decreased by a factor of 10 per 10 epochs
SIFNet [13]	CNN	Simulated data by neural mass models	cross entropy between predicted source region and label	Adam optimizer
ConvDip [14]	CNN	Simulated sinusoidal signal	weighted Hausdorff distance between predict source and label	Adam optimizer
DeepBraINNet [15]	RNN& LSTM	Simulated data	cross entropy	Backpropagation Through Time with the Nesterov method
DST-CedNet [8]	Encoder-decoder	Simulated data with time course derived from realistic E/MEG	$\lambda_1\ S_g - S_{re}\ _F^2 + \lambda_2\ S_g - S_{re}\ _{1,1} + \lambda_3\ X_g - X_{re}\ _F^2$	Adam optimizer, learning rate 10^{-4}
MS-ESI [16]	TCN & LSTM	Simulated data by neural mass models	$\ S_g - S_{re}\ _F^2$	Adam optimizer, learning rate 0.001
XDL-ESI [17]	Unrolled Optimization Neural Network	Simulated data	$\lambda_1\ S_g - S_{re}\ _F^2 + \lambda_2\ VS_{re}\ _{1,1} + \lambda_3\ MS - MS_{re}\ _F^2$	Not stated

S_g : ground truth of source activity, S_{re} : reconstructed sources, TCN: temporal convolution network, V/M : known transformation matrix, refer to [17] for detailed definition.

- dSPM: the i^{th} source is divided by $\text{tr}[L_i^\top(LL^\top + \lambda I)^{-2}L_i]$
- sLORETA: the i^{th} source is divided by $[L_i^\top(LL^\top + \lambda I)^{-1}L_i]^{\frac{1}{2}}$

The depth of each source dipole is modeled by the inverse of norm of lead-field matrix and scaled as follow: $D_i = [\text{svds}(LL^\top, 1)]^{0.5}/(L(:,i)^\top L(:,i))$, where D_i is the relative depth of i^{th} dipole, L is the lead-field matrix, $\text{svds}(X, 1)$ returns the largest singular value of X . The cortex is segmented into 4747 dipoles, and the channel number is 53. One source patch is generated for each dipole serving as the seed, and adjacent dipoles are included to reach an area approximating 2 cm^2 . Baseline activity is used to calculate the noise covariance for whitening. The results show that depth compensation strategies (implemented in MNE, dSPM and sLORETA) effectively reduce the bias, as indicated by the slope in linear regression analysis. Besides, sLORETA achieves the lowest DLE across various SNR, and LORETA yields the lowest SD in most cases.

IV. INFLUENCE OF BETWEEN-SOURCE CORRELATION AND FORWARD PROBLEM

In this section, the influence of between-source correlation on the performance of four aforementioned Minimum Norm (MN) methods and beamforming methods is evaluated. It is important to note that MN methods are insensitive to between-source correlation, whereas traditional beamforming methods,

such as LCMV, are significantly affected by source leakage from correlated activities. Recently, Cai et al. introduced a sparse Bayesian learning (SBL)-based LCMV approach designed to mitigate this leakage, which utilize SBL to learn the model covariance and subsequently construct the LCMV filter [12]. Consequently, the SBL-based LCMV was employed in this initial evaluation. Two distinct patches were selected to generate time series with varying correlation coefficients [0, 0.1, 0.3, 0.5, 0.7, 0.9]. The SNR is set at 20 dB and the area of each source is approximately 10 cm^2 . The time series within each patch were identical, and for each correlation level, time series were randomly generated 50 times. Performance metrics included SD (to evaluate spatial resolution), DLE (to evaluate localization error), and CORR (to evaluate temporal accuracy, specifically whether source leakage impacts the time course). The evaluation results (Fig. 4) indicate that the SBL-based LCMV is robust to between-source correlation, though the CORR metric showed a slight decrease at high correlation levels (e.g., >0.7).

The errors in the forward problem, related to the "inverse crime" in ESI performance evaluation, were assessed through simulation experiments utilizing different lead-field matrices for the forward and inverse problems. Specifically, the lead-field matrix for the forward problem was calculated based on the ICBM152 MRI template, with relative conductivities for scalp (=head), skull (=outer skull), and brain (=inner skull) set at 1, 0.0125, and 1, respectively. Three types of error in the forward problem are tested:

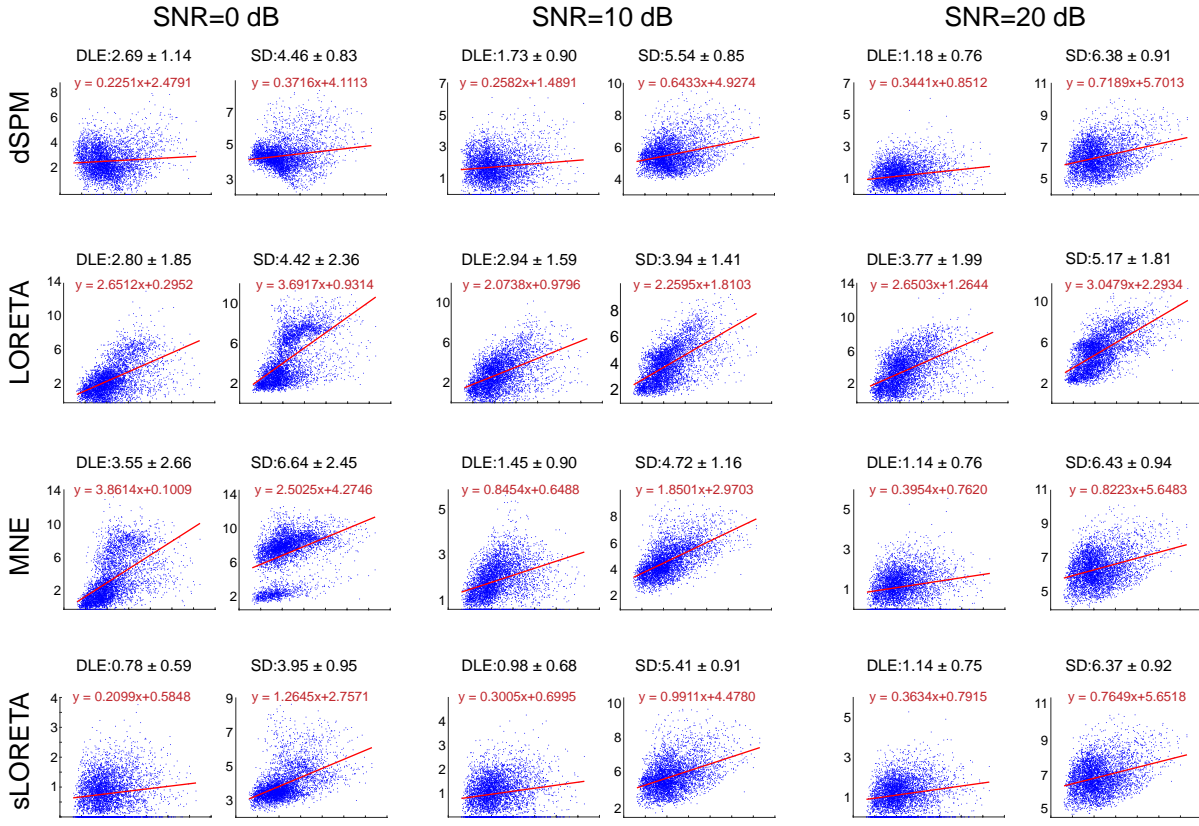


Fig. 3. Evaluation of depth-bias for four MN methods under various SNR levels.

- error in conductivity (C2): This involved using the same MRI template (ICBM152) but with different relative conductivities (relative conductivities = 1, 0.01, 1)
- error in geometry (C3): This involved using a different MRI template (FreeSurfer) with the same relative conductivities (1, 0.0125, 1)
- error in geometry and conductivity (C4): This involved using a different MRI template (FreeSurfer) and different relative conductivities (1, 0.01, 1).

Additionally, a case with no error in the forward problem (C1) was also tested. Simulations are repeated for 100 times. The results are presented in Fig. 5. Besides, it is found that the performance of all five methods decreased with errors in the forward problem. MNE, sLORETA, and dSPM were less affected by these forward problem errors.

REFERENCES

- [1] M. Dümpelmann et al., “sLORETA allows reliable distributed source reconstruction based on subdural strip and grid recordings,” *Hum. Brain Mapp.*, vol. 33, no. 5, pp. 1172–1188, 2012.
- [2] R. D. Pascual-Marqui et al., “Low resolution electromagnetic tomography: A new method for localizing electrical activity in the brain,” *Int. J. Psychophysiol.*, vol. 18, no. 1, pp. 49–65, 1994.
- [3] C. Cai et al., “Bayesian algorithms for joint estimation of brain activity and noise in electromagnetic imaging,” *IEEE Trans. Med. Imaging*, vol. 42, no. 3, pp. 762–773, 2022.
- [4] Z. Feng et al., “μ-STAR: A novel framework for spatio-temporal M/EEG source imaging optimized by microstates,” *NeuroImage*, vol. 282, p. 120372, 2023.
- [5] K. Liu et al., “VSSI-GGD: A variation sparse eeg source imaging approach based on generalized gaussian distribution,” *IEEE Trans. Neural Syst. Rehabil. Eng.*, 2024.
- [6] R. Sun et al., “Deep neural networks constrained by neural mass models improve electrophysiological source imaging of spatiotemporal brain dynamics,” *Proc. Natl. Acad. Sci. U. S. A.*, vol. 119, no. 31, p. e2201128119, 2022.
- [7] K. Sekihara and S. S. Nagarajan, *Electromagnetic brain imaging: A Bayesian perspective*. Springer, 2015.
- [8] G. Huang et al., “Electromagnetic source imaging via a data-synthesis-based convolutional encoder-decoder network,” *IEEE Trans. Neural Netw. Learn. Syst.*, 2022.
- [9] N. Otsu, “A threshold selection method from gray-level histograms,” *IEEE Trans. Syst. Man Cybern.*, vol. 9, no. 1, pp. 62–66, 1979.
- [10] F.-H. Lin et al., “Assessing and improving the spatial accuracy in MEG source localization by depth-weighted minimum-norm estimates,” *NeuroImage*, vol. 31, no. 1, pp. 160–171, 2006.
- [11] C. Cai et al., “Robust estimation of noise for electromagnetic brain imaging with the champagne algorithm,” *NeuroImage*, vol. 225, p. 117411, 2021.
- [12] C. Cai et al., “Bayesian adaptive beamformer for robust electromagnetic brain imaging of correlated sources in high spatial resolution,” *IEEE Trans. Med. Imaging*, vol. 42, no. 9, pp. 2502–2512, 2023.
- [13] R. Sun et al., “SIFNet: Electromagnetic source imaging framework using deep neural networks,” *bioRxiv*, pp. 2020–05, 2020.
- [14] L. Hecker et al., “ConvDip: A convolutional neural network for better EEG source imaging,” *Front. Neurosci.*, vol. 15, p. 569918, 2021.
- [15] J. C. Bore et al., “A long short-term memory network for sparse spatiotemporal EEG source imaging,” *IEEE Trans. Med. Imaging*, vol. 40, no. 12, pp. 3787–3800, 2021.
- [16] Z. Yu et al., “Electrophysiological brain imaging based on simulation-driven deep learning in the context of epilepsy,” *NeuroImage*, vol. 285, p. 120490, 2024.
- [17] M. Jiao et al., “XDL-ESI: Electrophysiological sources imaging via explainable deep learning framework with validation on simultaneous EEG and iEEG,” *NeuroImage*, vol. 299, p. 120802, 2024.

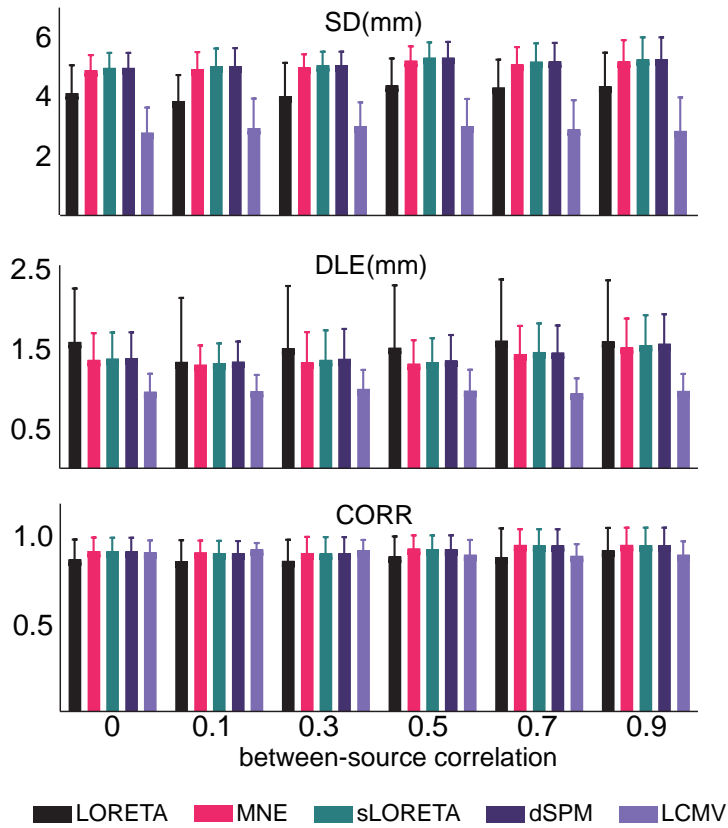


Fig. 4. Performance metrics of five ESI methods across varying between-source correlations. Two source patches are generated and the area of each source is around 10 cm^2 . The SNR is set at 20 dB. Results are presented as mean and standard deviation.

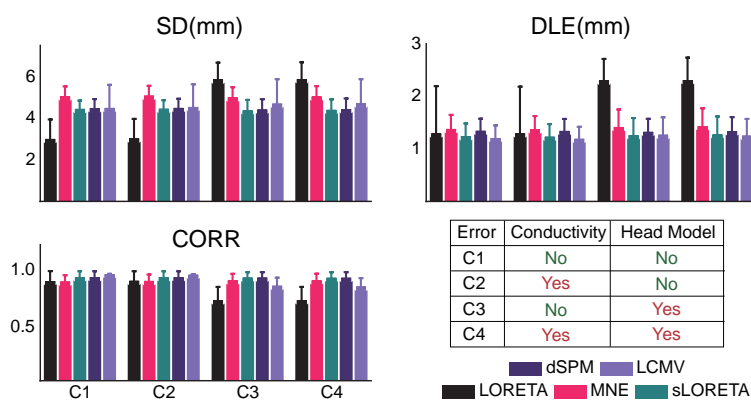


Fig. 5. Performance metrics of five ESI methods across different types of forward error. C1: no error; C2: error in conductivity; C3: error in geometry; C4: error in both geometry and conductivity. Results are presented as mean and standard deviation.